28

Investigations of Supersonic Flow around a Long Axisymmetric Body

M.R. Heidari, M. Farahani, M.R. Soltani and M. Taeibi-Rahni
Garmsar Branch of Islamic Azad University,
Sharif University of Technology
Iran

1. Introduction

One of the most important parameters affecting missiles' length and diameter is the required space for their apparatus, systems, etc. Increasing this space causes an increase in both the body length and the missile's fineness ratio, L/d (Fleeman, 2001). For such bodies, the problems of flow separation and boundary layer growth at various flight conditions are very important. Of course, the boundary layer growth and its separation, affect the aerodynamic characteristics, particularly the drag force and the stability criterion. Both of these have important roles in the missile performance and its mission implementations. Also, the performance of various control surfaces (especially those located close to the end of the body) varies with flow separation (Cebeci, 1986).

For some rockets and missiles, the after body cross-section changes longitudinally (particularly in space vehicles). Furthermore, due to the lack of sufficient space for arranging the systems (e.g., actuator of controlled fins, avionics, etc.), it is necessary to increase the body cross section near those systems. The lack of space may also appear when controlled fins are installed on the motor surface. Hence, in many occasions the body cross-section needs to be increased (Chin, 1965; Soltani et al., 2002).

However, the computation of the flow parameters and their variations for non-zero angles of attack, when bodies are tapered, is not an easy task, e.g., it takes a considerable amount of memory and CPU time to compute the flow over such bodies. In addition, as the angle of attack increases, the flow over a portion of the body may separate, making the flow more complicated. Moreover, experimental data for flow properties along tapered bodies to validate CFD codes are rare (Soltani et al., 2002; Perkins & Jorgensen, 1975).

The computational simulation of flow over complex geometries usually requires structured multi-block grids. On the other hand, the geometric complexity requires more blocks and also more grid points. Even though, the computer programming (using multi-block grid for such flows) is very troublesome, it is computationally very efficient and quick. On the other hand, suitable grid generation plays the first and the most important role, when using multi-block grid.

Grid generation needs to be consistent with flow solution. In some methods, the discritization error increases due to the inaccurate adoption of the grid boundaries with the real flow boundaries, which could be due to the non-orthogonality of the grid lines, especially near the walls.

There have been many research performed on the areas of generation and use of multi-block grids, grid generation techniques, data management methods in different blocks, production of grid generation softwares which optimally require less trained users, and quicker grid generation, especially for complex geometries (Amdahl, 1988; Sorenson & McCann, 1990).
The different steps to compute the flow using multi-block grid are: 1. geometric recognition and setting a suitable block structure, 2. grid generation inside each block and finding the nodes on the block boundaries, and 3. solving the flow inside each block and then in the whole domain. Also, multi-block grid generation has four steps, namely, dividing the flow domain into different blocks, determining the exact geometric characteristics of each block, grid generation in each block, and optimization of the overall grid (Boerstoel et al., 1989). The situation and the location of the boundaries between the blocks are very important and thus an inefficient structuring can lead to the divergence of the overall solution. The flow physics, such as shock waves and separated flow regions, determine the required number of blocks and how they are distributed.
In the present work, a series of wind tunnel tests on a long axisymmetric body were performed to investigate the pressure distribution, the boundary layer profile, and other flow characteristics at various angles of attack and at a constant supersonic Mach number of 1.6. Because of low maneuverability of high fineness ratio missiles, the range of angles of attack for the present study was chosen to be moderate. Then, the effects of the cross sectional area variations on the surface static pressure distribution and on the boundary layer profiles were thoroughly investigated. This was performed by installing two belts (strips) having different cut-off angles on the cylindrical portion of the model. One of these belts was installed at the beginning of the after body part (x/d=7.5), while the other was located near the end (x/d=13.25). By changing the belt leading edge angles, different bodies were generated and thus the effects of varying the body cross-section were studied.
In the numerical part of this work, a stationary turbulent supersonic axisymmetric flow over the same body at zero angle of attack (in the absence of body forces and heat sources) was investigated using the computer code developed in this work (MBTLNS). Adiabatic wall with negligible variations of the viscous fluxes in the streamwise direction was assumed. Also, the flow domain was blocked in streamwise direction and patched method was used in the block boundaries. In each block, the thin layer Navier-Stokes (TLNS) equations were solved, using the implicit delta form finite difference method with Beam and Warming central differencing scheme (Beam, & Warming, 1978). For turbulence modeling, the algebraic two-layer Baldwin-Lomax model was used and the shock waves were captured using shock capturing technique. In each iteration of the overall solution, the flow domain is swept from the first block at the nose to the last block at the end of the body. The computational results for zero angle of attack, Mach number of 1.6, and Reynolds number of 8×106 for flow over an axisymmetric ogive-cylinder with two sets of strips with angles 5 and 15 degrees were compared with the related experimental results obtain in this work. The most important ability of the present software is that, it can solve the flow around complex geometries, using a personal computer with relatively small memory.

2. Experimental equipments and tests

All tests were conducted in the trisonic wind tunnel of QRC. The equipments used for this investigation include: Schlieren visualization system, A/D board, traversing mechanism, rake, vacuum pump, manometer, computer, data acquisition software, pressure transducer, and multiplexer board.

The QRC wind tunnel is an open-circuit blow down tunnel and operates continuously between Mach numbers 0.4-2.2, via engine RPM and nozzle adjustments. It has a test section of 60×60×120 cm3 and is equipped with various internal strain gauge balances for force and moment measurements, pressure transducers, Schlieren visualization system, etc. (Masdari, 2003).

The model used in this study had a fineness ratio of 2.5 and a circular-arc, ogival nose tangent to a cylindrical after body with L/d=15 (Fig. 1.a). It was equipped with 36 static pressure ports located both longitudinally and circumferentially. To study the effects of cross section changes, two belts with various leading edge angles were installed on the model (Fig. 1.b). Here, the first model is used when talking about the main or simple model (the one without belts), the second model for the one with (5, 5) degrees belts, and the third model for the one with (15, 12) degrees belts.

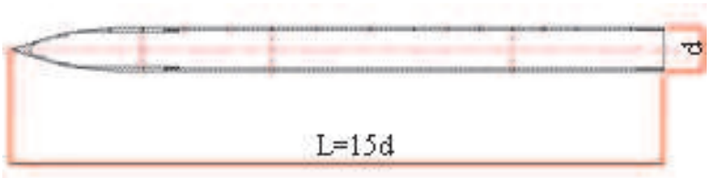

a) Simple model

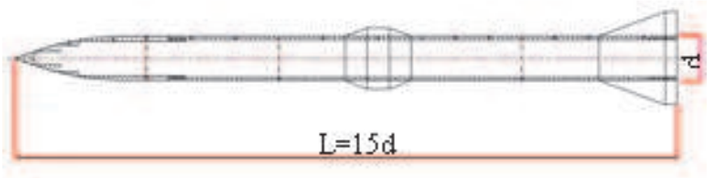

b) Model with belts

Fig. 1. Schematic of different models used.

The traversing mechanism, which was designed and built particularly for this study, is capable of moving the rake perpendicular to the body axis with small steps of about 0.003 mm in z direction. This system was installed on the α-mechanism base such that, the tubes (pitot total pressure) of the rake were always parallel to the model. Note, the entire traversing mechanism was fully controlled by a computer.

Various tests were conducted to study the flow characteristics along the model. The free stream Mach number was 1.6, while the angle of attack was varied between -2 and 6 degrees. At each angle of attack and for all models, the rake at several longitudinal stations for at least 11 locations in z direction obtained the total pressure data. An accurate linear potentiometer was used to determine the distances between the body surface and the rake. Note, all experimental data shown here are ensemble averaged of several hundred data taken several times to ensure repeatability.

3. Governing equations and computational methodology

In the present study, a turbulent supersonic flow over a long axisymmetric body at zero angle of attack was computationally simulated. The Reynolds averaged TLNS equations were solved using Beam and Warming central differencing and Baldwin-Lomax turbulence model. This model is frequently used, because of its simplicity and its reliability. Even

though in some flow situations, it is up to about 10% less accurate compared to some other models, it can reduce the amount of computations up to about 50%.

The first step in grid generation is the correct nodal distribution along the body surface. Then is the blocking of the domain and finally comes the grid generation inside each block. Since we are not ignoring the viscosity, much finer grid is required near the surfaces. Also, finer grid is required in the block which may contain shock waves, flow separation, or other high flow gradient regions. For most blocks, where there are relatively simple geometries, algebraic grid generation is usually used.

The location of the block interfaces is very important. In this work, the blocks were structured in the streamwise direction. For blocking of the domain, one needs to first estimate different flow phenomena and the complexity of the body geometry, which may encounter. Then, the block interfaces are located. Here, we used connected and disconnected uniform patched method at the interfaces. Note, whenever connected meshes are used, the lines from one block are continued into the next block. This way, interpolation is not usually required at the interfaces. Besides the limitations this may bring along, it eliminates the errors due to non-conservative data along the interfaces.

Even when continuous grid (same grid type in each block) is used, any sudden change along the block interfaces (such as angles between the lines of the two neighboring blocks) may cause drastic discontinuity of the grid transformation metrics. On the other hand, for more accurate application of the wall boundary conditions and the flow solutions in each block, it may be required to increase the number of nodes and the grid lines, especially in the direction perpendicular to the wall. This usually leads to disconnected grid at the interfaces. Mostly, this is done by halfing or doubling the grid points in the blocks neighboring the interfaces (Bohbot et al., 2000).

In each block, the boundary conditions and the information received from the neighboring blocks affect the flow solution. Thus, any error related to the transfer of information within the blocks directly affects the solution in each block and the overall solution and its convergence. Therefore, we need to use interpolation techniques at the interfaces with the least error, which is preferably conserved.

In the present work, a suitable linear interpolation technique was used for computations at points of a block extended into the neighboring block. Thus, the distribution of lines in the left and the right sides of the interfaces is quite arbitrary and without any limitations. After breaking down the flow domain into several blocks, the information set for each block is obtained. This set includes the block number, the interface numbers and types, the geometric locations of the corners of each block, and the numbers and types of the neighboring interfaces. Also, other internal information of each block, such as the number of the nodes and their arrangements, the CFL number, the artificial viscosity coefficient, etc., have to be known, before the flow solution is performed.

Even though, the solution may be converged in each block, the overall solution may well be diverged. This difficulty mainly arises from the inappropriate ordering of the solution procedure for different blocks, which needs to be simple and smooth. Also, it is very important that, different flow variables have the same weight and harmony. In this work, using a simple and suitable procedure, we start from the first block at the nose, which contains the upstream inflow information, and pass though the chain of the blocks, until we reach the last one, located at the end of the body, containing the outflow information. In each block, the solution is only performed in one time step. Note, if we were having any type of iterations in any block, it should be harmonized with the other blocks, especially the

neighboring ones. This is a considerably difficult task and can lead to convergence problems of the overall solution.
Here, the solution accuracy has been compared to the single block case. As far as the convergence speed is concerned, different parameters, such as the numbering and the arrangement of the nodes, the CFL number, the initial conditions, the time step, the artificial viscosity coefficient, etc. for each block, and the position and type of block interfaces have been thoroughly investigated and evaluated.

4. Results and discussion

A supersonic turbulent flow over a long axisymmetric body was investigated both experimentally and computationally. The experimental study consisted of a series of wind tunnel tests for the flow over an ogive-cylinder body at Mach number of 1.6 and at angles of attack between -2 and 6 degrees. To study the effects of the cross section variations on the pressure distribution and on the boundary layer profiles, several belts with various leading edge angles were installed at different locations along the cylindrical portion of the model. The wind tunnel tests included the surface static pressure and the boundary layer profile measurements. Further, the flow around the model was visualized using Schlieren technique. All tests were conducted in the QRC's trisonic wind tunnel. On the other hand, for the above body, a 1.6 Mach number and a 8×106 Reynolds number flow at zero angle of attack was computationally investigated, using a multi-block grid (with patched method around the block interfaces) to solve the TLNS equations. The numerical scheme used was implicit Beam and Warming central differencing, while Baldwin-Lomax turbulence model was used to close the RANS equations.
First, at various angles of attack, the Schlieren visualization technique was used to study the shape of the shocks formed around the model nose and places where the area changed (and their variations with angle of attack). Figure 2 shows the shock waves, as well as the expansion waves, on the large strip at zero angle of attack. The related numerical results are also shown there for comparison purposes. From this figure, it is seen by inspection that, there exists relatively close correlations between the numerical and the experimental results for both cases.

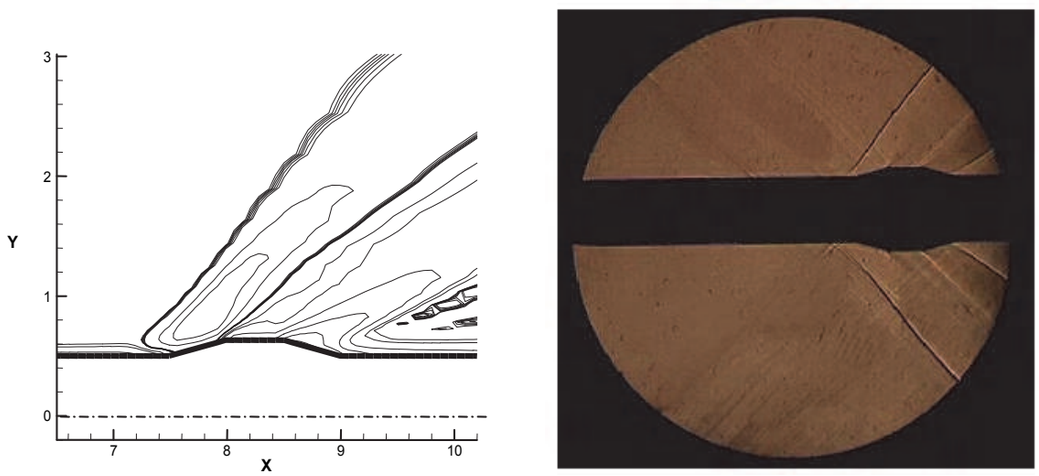

a) Numerical b) Experimental

Fig. 2. Experimental and numerical flow field over the model with large belt (15°) at $\alpha = 0$.

Figure 3 shows the shock wave formed in front of the model and ahead and behind the belt used for varying the model cross section at 6 degrees angle of attack. It is seen from this figure that, the shock wave is not symmetric resulting in a lower strength on the leeward side of the model causing higher pressure on the windward portion of the nose and lower pressure on its leeward side (thus, a normal force is generated). Figure 3.b clearly shows the oblique shock, as well as the expansion waves, formed in the front and on the surface of the belt installed at x/d=7.5. Furthermore, the oblique shock formed behind the belt to reduce the flow velocity and to turn it parallel to the model surface is clearly visible in this figure. Again, the strengths and the shapes of upper and lower shock formed ahead of the belt are not the same.

Figure 4 shows the longitudinal static pressure distribution over the model surface. Figure 4a compares our experimental and CFD results for zero angle of attack, while Fig. 4b compares our experimental results with theoretical ones (SOSE; Second Order Shock Expansion) for 4 and 6 degrees angle of attack (Moore, 2000). Note, the measurement errors are calculated and shown in Fig. 5b. From these figures, it is clearly seen that all three methods predict the surface pressure very closely for 0<L/d<12 at $\alpha = 0$ degree. From Fig. 4.b the experimental and the theoretical data compare well up to about x/d=12. The differences are probably due to the base flow affecting the boundary layer on the model surface near its end. Note that, by increasing the angle of attack, the pressure taps located at zero circumferential angle ($\theta = 0$) will be located at the leeward side of the model. Therefore, their static pressure should decrease. These pressure losses are however considerable only along the nose section of the body. This confirms that, for axisymmetric bodies, the contribution of the nose in generating the lift force is greater than that of its after body portion (Soltani et al., 2004, 2005; Heidari et al., 2005). Increasing α from 4 to 6 degrees has small effects along the nose section.

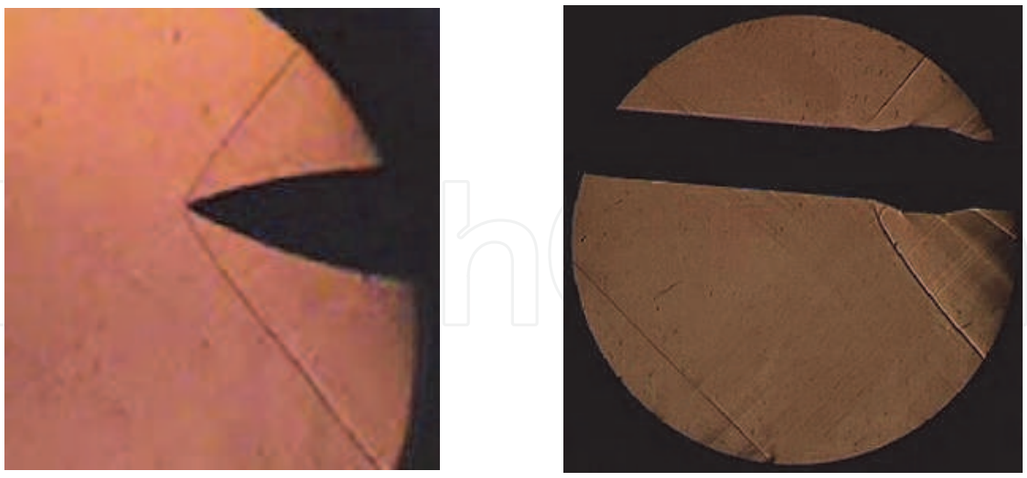

a) Oblique shock in the nose region of the model

b) Compression and expansion waves around the large belt (15°)

Fig. 3. Schlieren photograph illustrating the shock formation at $\alpha = 6^\circ$.

The experimental and the theoretical circumferential pressure data at x/d=3 and 11.5 for 4 and 6 degrees angles of attack are shown in Fig. 5. For the first station, by increasing the

angle of attack, Cp increases slightly at the windward side, as expected. As α increases, the vortices separate from the nose and extend to the end of the body. These vortices in Fig. 5b are in general asymmetric and cause asymmetry of the circumferential pressure distribution on the leeward side of the body (Moore, 2000). In addition, the sensitivity of the model installation is high due to its large fineness ratio; hence a small error can cause a considerable sideslip angle. Note, the flow field study showed that, the flow has a small yaw angle too (Masdari, 2003).

Figure 6 shows the grid, the velocity vector field, and the pressure and density contours for flow over the small belt model at zero angle of attack, Mach number of 1.6, and Reynolds

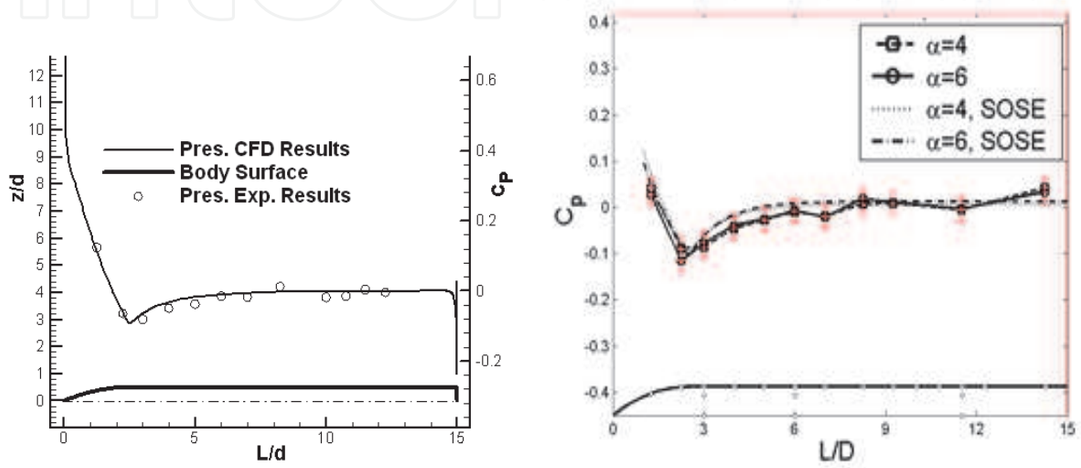

a) $\alpha = 0$ b) $\alpha = 4^{\circ}$ and 6°

Fig. 4. Comparison of experimental, theoretical, and numerical longitudinal pressure distribution.

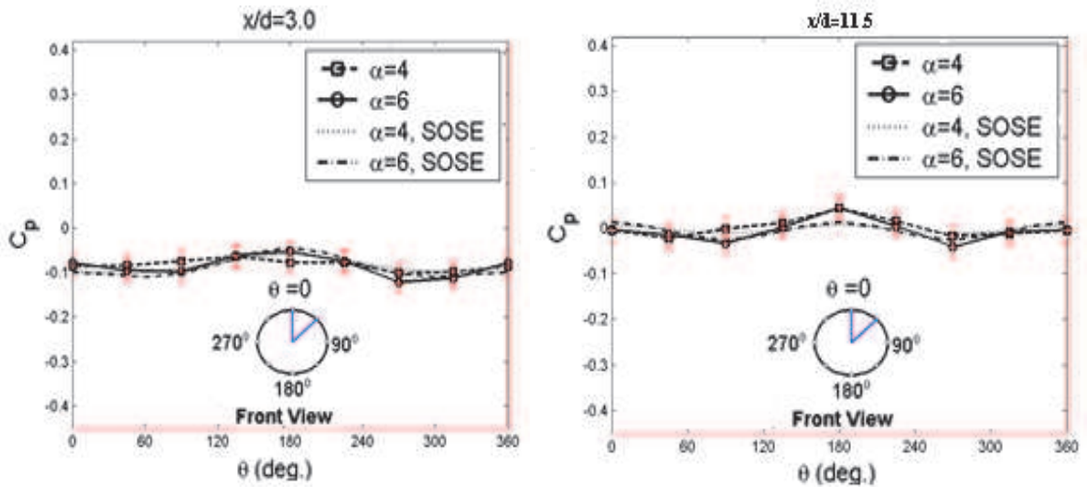

a) x/d=3 b) x/d=11.25

Fig. 5. Comparison of experimental and theoretical circumferential pressure distribution at $\alpha = 4^{\circ}$ and 6°.

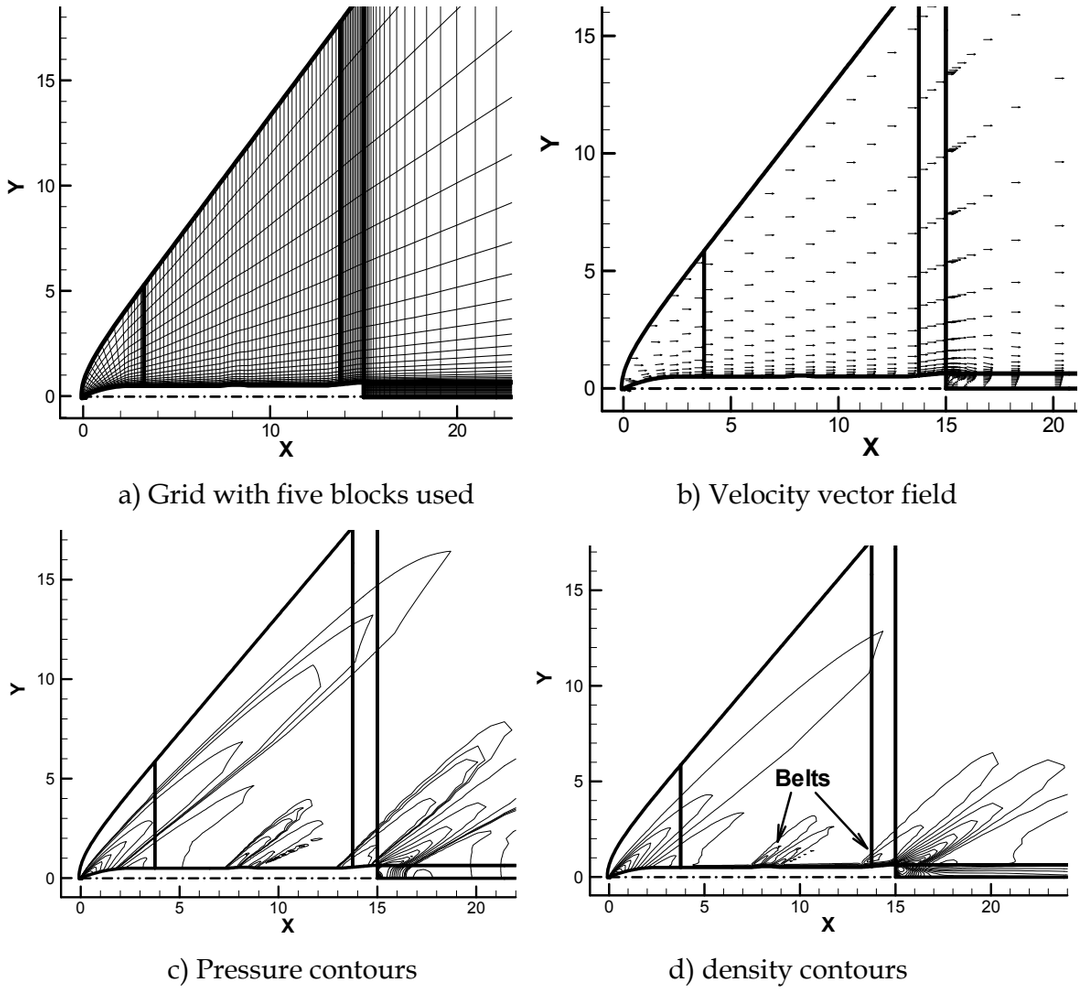

a) Grid with five blocks used b) Velocity vector field

c) Pressure contours d) density contours

Fig. 6. Experimental Flow around the model with small 5° belt.

number of 8×10^6 (described before). Not, the flow domain has been broken into five blocks. Also, note from the pressure and the density contours that, the solution is very smooth and continuous at the block interfaces. In all these solutions, the optimal grid has been determined and used. Also note that, the bow shock near the body nose has been captured with suitable accuracy and other flow shock and expansion waves along with the flow vortices have been shown near the belts.

The effect of varying the model cross section (by adding belts with different leading edge angles) and the circumferential pressure distribution at 6 degrees angle of attack are shown in Fig. 7. The computational drag coefficient is obtained from the viscosity and pressure gradient effects on the body surface. Here, the longitudinal pressure distribution for both the numerical and the theoretical predictions compared well with the experimental data up to the location where the model frontal area was changed via the belt. Behind the belt however, all results are almost identical. The presence of the belt increases the longitudinal surface pressure by formation of an oblique shock as seen in Fig. 3.b over the inclined part of the belt. However, around the surface of the belt and behind it, the pressure decreases due to the formation of the expansion waves (also seen in Fig. 3.b). The results of the circumferential pressure

distributions show that, sudden changes in cross sectional area have small effects on the pressure distribution around the perimeter of the model behind the belt (Fig. 7.b).

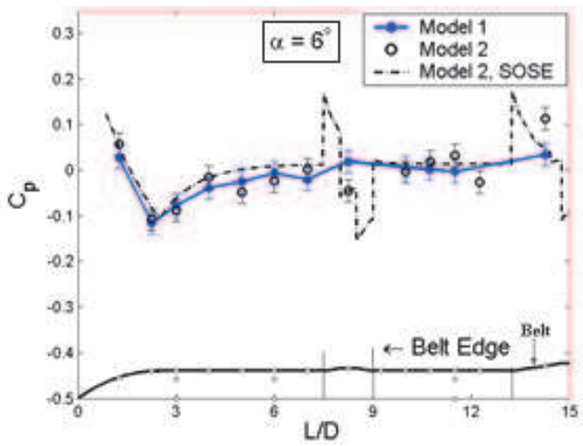

a) Experimental, theoretical, and numerical longitudinal pressure distribution.

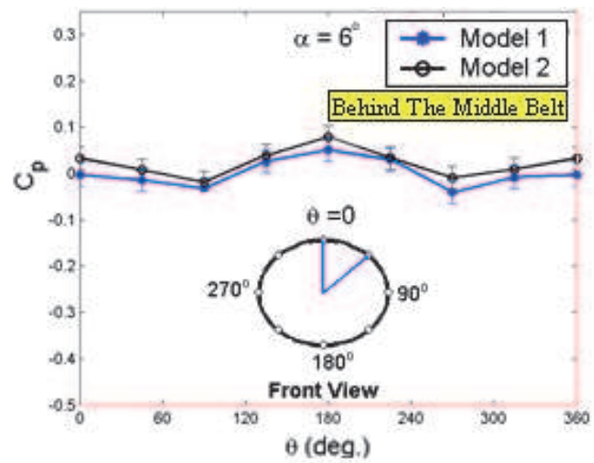

b) Circumferential pressure distributions behind the middle belt (x/d=11.25).

Fig. 7. Effect of cross section variations on the model pressure distribution (model 2).

The drag coefficient is obtained from shear viscosity and pressure gradient effects on the body surface. In this work, for the small belt model, a wave drag of 0.223, a friction drag of 0.071, and a base drag of 0.369 have been computed (thus, the total drag was 0.663). The drag coefficients for all models are shown in Table 1.

Model	Middle Belt Angle (Deg.)	End Belt Angle (Deg.)	Wave Drag	Friction Drag
Body Alone	-	-	0.146	0.077
Body with Small Belts	5	5	0.223	0.071
Body with Big belts	15	12	0.776	0.068

Table 1. The drag coefficients for the three cases studied.

The computational and the experimental boundary layer profiles for the simple model (uniform cross section) were compared at three different longitudinal stations and at zero angle of attack in Fig. 8. From this figure, the agreements of data are relatively close, particularly for z<7 mm.

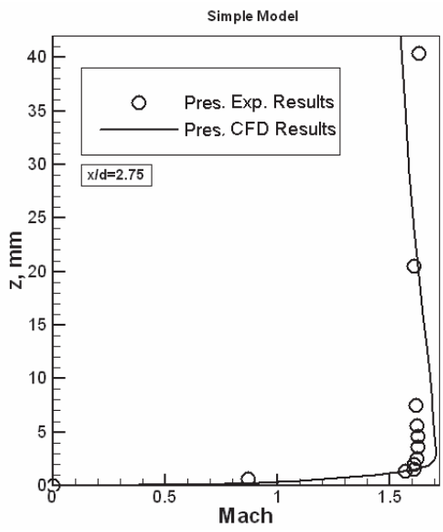

a) x/d=2.75

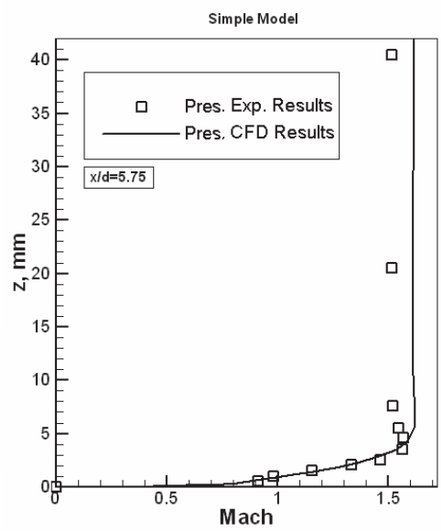

b) x/d=5.75

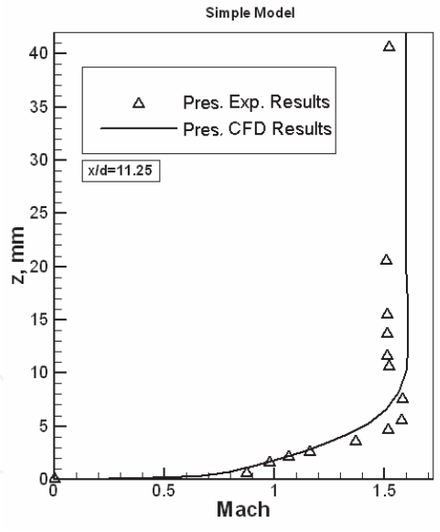

c) x/d=11.25

Fig. 8. Experimental and numerical boundary layer profiles for simple model at $\alpha = 0$.

Figure 9 shows the boundary layer profiles above the model at three different stations: x/d=2.75, 5.75, and 11.25 for two different angles of attack (0 and 6 degrees). From this figure, it is clearly seen that the boundary layer thickness increases, with x/d. Further, this figure shows that for x/d=2.75 and at $\alpha = 6^{\circ}$, the velocity at the edge of the boundary layer ($z \cong 5$ mm) is slightly higher than that outside of it ($z \cong 18$ mm). While, for other locations

(x/d=5.75 and 11.25) the velocity outside the boundary layer never reaches that of V_∞ at M_∞ =1.6. The increased velocity at the boundary layer edge is related to the increase in the mass flow rate at the outer portion of the boundary layer due to the velocity reduction in the inner layers (entrainment). Since the decrease in the velocity inside the boundary layer causes lower mass flow rate there, it must be compensated by an increase in the velocity at the edge of the boundary layer.

At $\alpha = 6^\circ$ and at x/d=11.25, the value of $\partial M / \partial z$ is different in comparison with the other data shown in Fig. 9.b. This change is probably due to the separation of the body vortices (Jorgensen & Perkins, 1955). Moreover, the growth of the boundary layer at x/d=11.25 is greater than that of the other stations (e.g., x/d=2.75 and 5.75). Note, for all three stations, as the x increases, the boundary layer thickness increases considerably. However, the increase in the velocity at the boundary layer edge decreases marginally. This increase is due to the growth of the momentum layer thickness, δ^*, which permits the required mass flow rate through the boundary layer (Heidari et al., 2005).

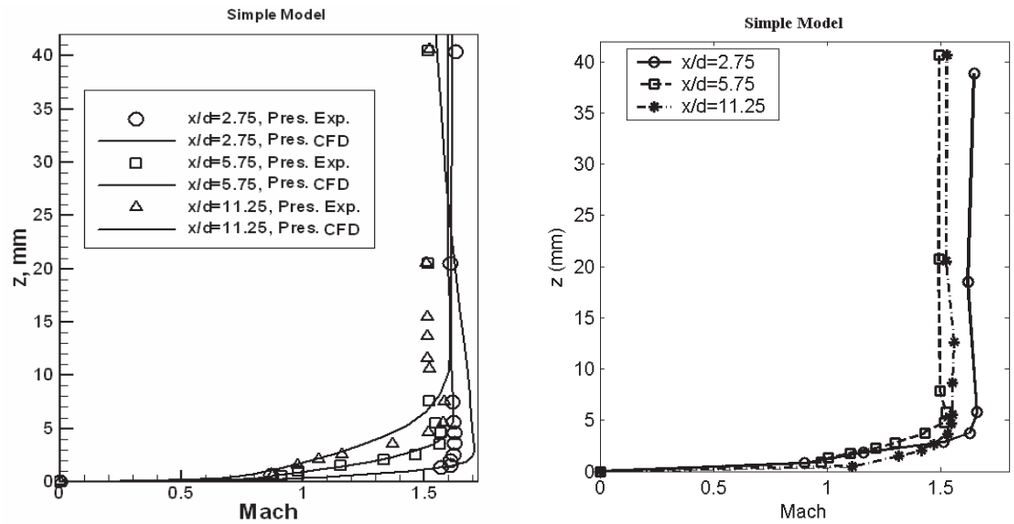

a) $\alpha = 0$ b) $\alpha = 6^\circ$

Fig. 9. Comparison of the boundary layer profiles around the body.

The variations of the experimental boundary layer Mach numbers for the simple model at x/d=5.75 and 11.25 (at various angles of attack) are shown in Fig. 10. At x/d=5.75. With increasing the angle of attack, the boundary layer thickness grows. However, a slight increase in the boundary layer thickness is noted for small angles of attack. At higher angles of attack, the boundary layer thickness decreases appreciably for x/d=11.25. It is presumed that, the boundary layer fluid is shifted to form a pair of vortices along the sides of the model at large α, hence reducing the boundary layer thickness.

The comparison of the numerical and the experimental boundary layer profiles over model 2 ahead and behind the middle belt at zero angle of attack is shown in Fig. 11. This data compares relatively well, especially for x/d=5.75. Note, the differences between the CFD and experimental results obtained are at most 15%. However, it is noted that such difference is much less (less than 7%) in other figures.

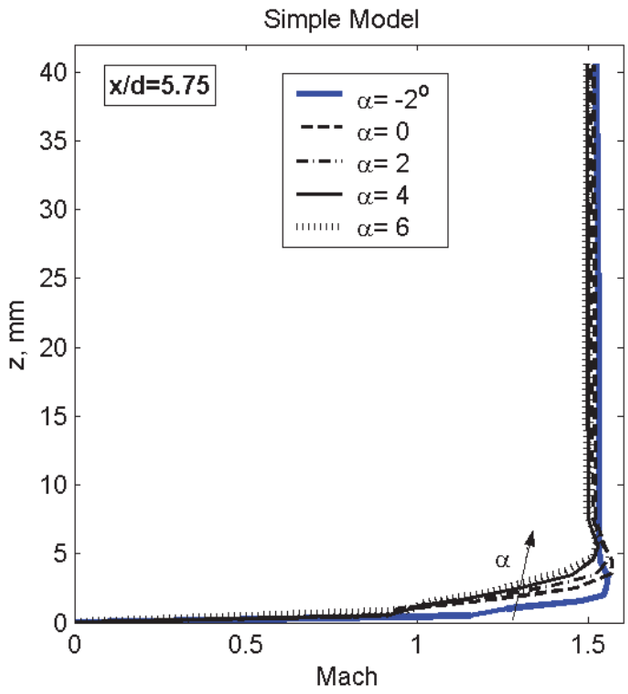

a) x/d=5.75

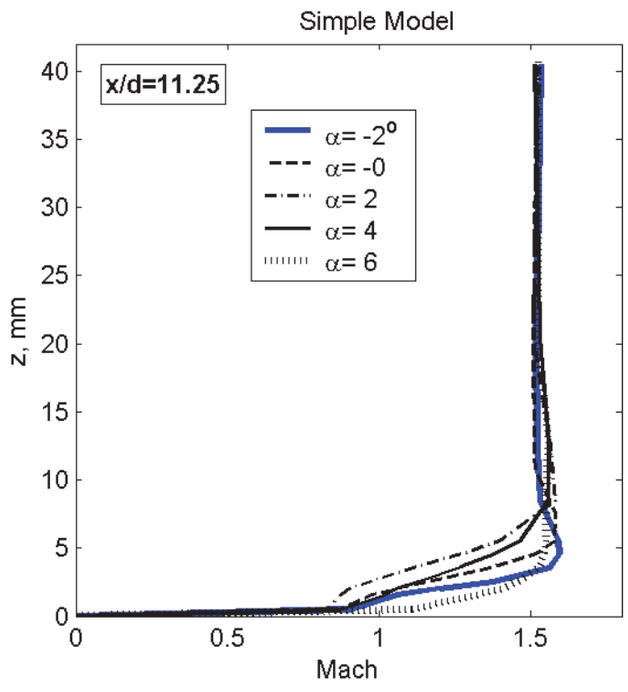

b) x/d=11.25

Fig. 10. Effects of angle of attack on boundary layer profiles.

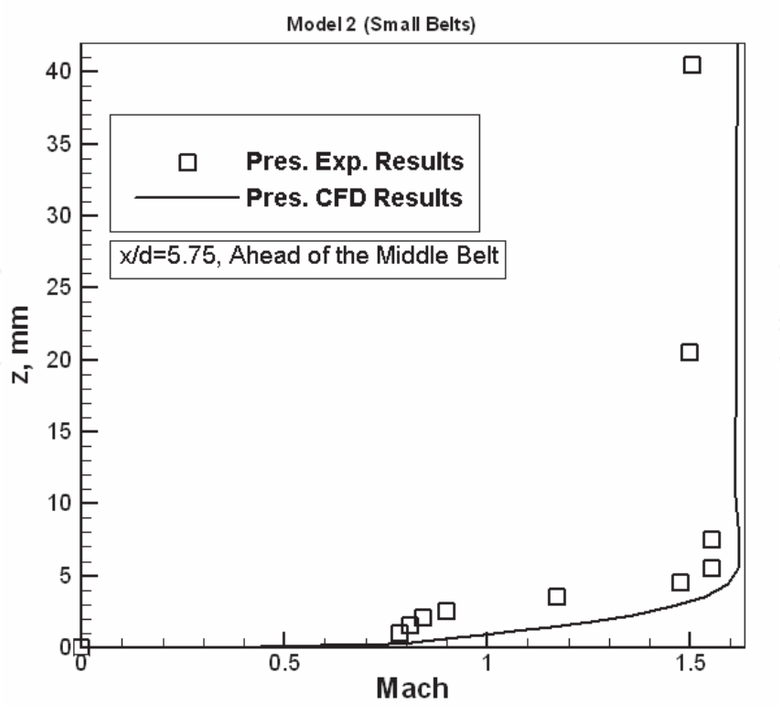

a) x/d=5.75

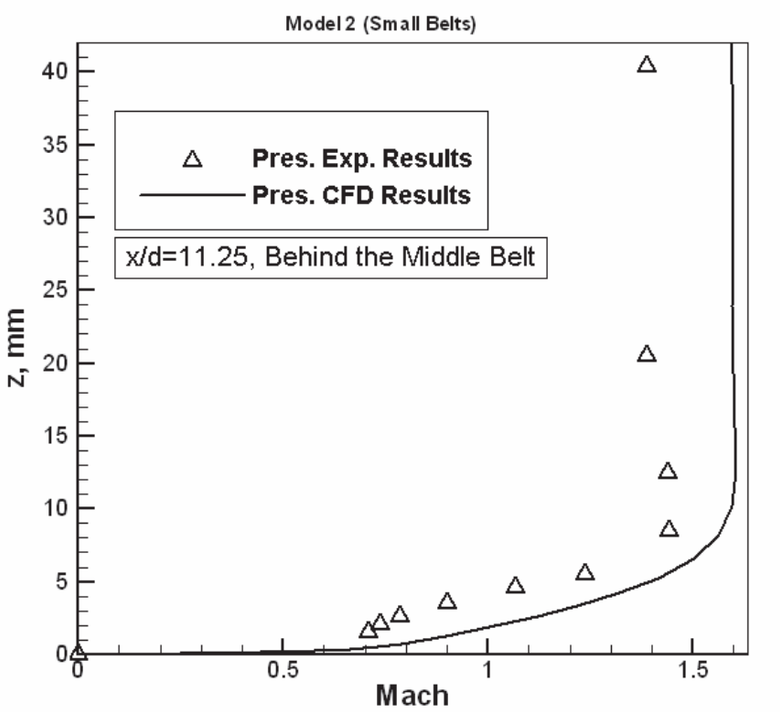

b) x/d=11.25

Fig. 11. Experimental and numerical boundary layer profiles for model 2 at $\alpha = 0$.

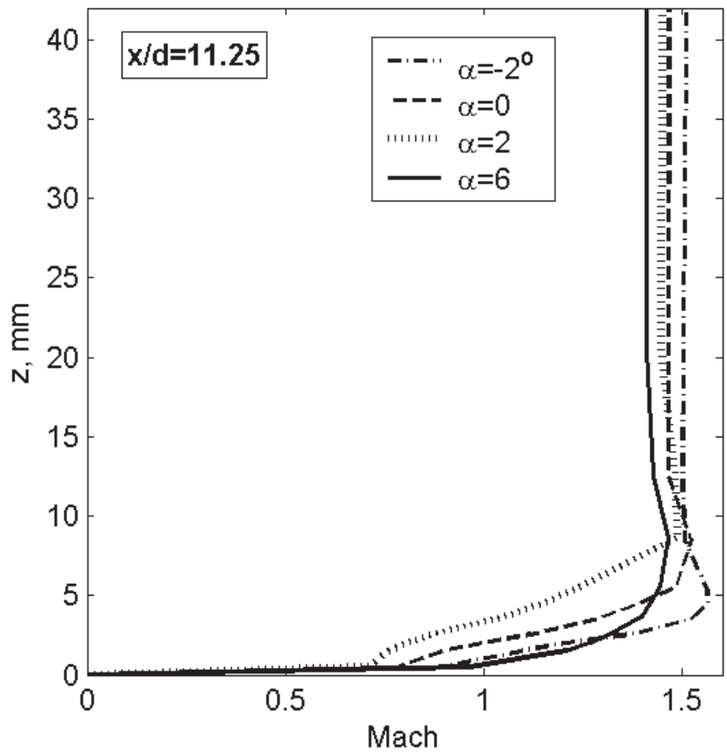

Fig. 12. The effects of angle of attack on boundary layer profiles for model 3.

The variations of the experimental Mach number in the boundary layer for model 3 at x/d=11.25 at various angles of attack are presented in Fig. 12. The trend of the boundary layer profiles for this model is the same as the simple model (Fig. 10.b). With increasing the angle of attack up to 2°, a slight increase in the boundary layer thickness is noted, while at higher angles of attack, the boundary layer thickness decreases appreciably. Note, the presence of the belts has almost no effect on the variations of the boundary layer profiles with angle of attack.

5. Conclusion

An extensive experimental study on a long axisymmetric tapered body in a turbulent supersonic flow was performed to mainly investigate the pressure distributions and the boundary layer profiles at various angles of attack. In order to study the effects of the model cross section variations, several belts with various leading edge angles were installed at different locations along the cylindrical portion of the model. In addition, the same flow at zero angle of attack, using structured multi-block grid (with patched method at the block interfaces) and Baldwin-Lomax turbulence model, solving the TLNS equations, was computationally simulated.

The experimental static surface pressure results show that, the circumferential pressure at different nose sections vary significantly with angle of attack (in contrast to the circumferential pressure signatures along the cylindrical part of the body). On the other hand, the total pressure measurements in the boundary layer vary significantly both radially and longitudinally.

Also, the experimental results obtained indicate that, the installation of the belts with various leading edge angles has little effects on the pressure distributions along the forebody, while it has considerable effects on the after body pressure signatures. Also, the belts affect the boundary layer profiles, increasing their thicknesses and changing their shapes. Note, for the models with belts, the value of $\partial M / \partial z$ at z=0 is considerably different.

The computational results obtained were compared to some of our related experimental data showing relatively close agreements. Note, at the block interfaces, there are not shown to be any noticeable discontinuities. Also, the flow shock and expansion waves are clearly shown in our numerical results and the computational shock angles compare well with the Schlieren results. These indicate suitable accuracy of our numerical methodology. The Mach number contours at 6° angle of attack showed vortices at the end of the body. It seems that, the addition of the belts increases the strength of these vortices and makes them more symmetric. It was also demonstrated that, for the same number of grid points, the single block case requires much more memory than the multi-block cases. The MBTLNS computer code obtained during this research is considerably robust, fast, and applied; it can be used for many other axisymmetric complex geometries.

According to table 1, the drag coefficient, as an important performance quantity, is reduced with decrease in the belt angle. Also, for high belt angles, not only drag, but the lift coefficient is reduced due to flow separation downstream of the belt. Note, as far as design is concerned, it is hard to make major conclusions, since we have only studied this problem from a certain points of view.

6. Nomenclature

a	Speed of Sound
D	Body Diameter
L	Body Length
M	Mach Number
x	Longitudinal Distance from the Nose
z	Perpendicular Distance from the Body Surface
C_p	Pressure Coefficient
L/d	Fineness Ratio
α	Angle of Attack
θ	Circumferential Angle

7. References

Amdahl, D.J. (1988). Interactive Multi-Block Grid Generation, Numerical Grid Generation in Computational Fluid Mechanics, *Eds.* S. Sengupta, J. Hauser, P. R. Eiseman and J. F. Thompson, Pineridge Press, pp. 579-588

Beam, R.M. & Warming, R.F. (1978). An Implicit Factored Scheme for the Compressible Navier-Stokes Equation, *AIAA Journal*, Vol. 16, No. 4, pp. 393-402

Boerstoel, J.W.; Jacobs, A.; J.M. & Kassies. (1989). Design and Testing, Norway

Bohbot, J.; Bertin, D. & Darracq, D. (2000). A Conservative Patched Grid Algorithm for Turbulent Flow Computations of 3-D Complex Configurations, *European Congress*

on Computational Methods in Applied Sciences & Engineering, ECCOMAS 2000, Barceiona, 11-14 September 2000

Cebeci, T. (1986). Three Dimensional Boundary Layer on Missiles, *Tactical Missile Aerodynamics*, Vol. 104, pp. 723-777

Chin, S.S. (1965). Missile Configurations Design, McGraw-Hill

Fleeman, E.L. (2001). Tactical Missile Design, *AIAA Education Series*, AIAA, New York

Heidari, M.R.; Soltani, M.R.; Farahani, M. & Taeibi-Rahni, M. (2005). Experimental Investigations of Supersonic Flow around a Long Axisymmetric Body, *Esteghlal Journal of Engineering*, ISSN 1025-2851, Vol. 24, No. 2, pp. 171-192

Jorgensen, L.H. & Perkins, E.W. (1955). Investigation of Some Wake VortexCharacteristics of an Inclined Ogive-Cylinder Body at Mach Number 2, NACA-RM A55E31

Masdari, M. (2003). The Flow Study in the Test Section of the Trisonic Wind Tunnel of Qadr Research Center, *M.Sc. Thesis, Aerospace Engineering Dept*., Sharif Univ. of Technology, Tehran, Iran

Moore, F.G. (2000). Approximation Methods for Weapon Aerodynamics, Progress in Astronautics and Aeronautics, *AIAA Journal*, ISSN 1-56347-399-2, Vol. 186, Reston, VA 20191-4344 USA

Perkins, E.W. & Jorgensen, L.H. (1975). Comparison of Experimental and Theoretical Normal-Force Distributions (Including Reynolds Number Effects) on Ogive-Cylinder Body at Mach number 1.98, NACA-TN 3716

Soltani, M.R.; Fazeli, H. & Farhanie, B. (2002). Experimental Investigations of Aerodynamic Behaviors of Two Wrap Around Fins, *Esteghlal Journal of Engineering*, ISSN 1025-2851, Vol. 21, No. 1, pp 141-152

Soltani, M.R.; Taiebi-Rahni, M.; Farahani, M. & Heidari, M.R. (2004). Experimental Investigations of Surface Pressure Distributions and Boundary Layer Profiles around a Long Axisymmetric Body with Varying Cross Section, IMECE2004, Kuwait

Soltani, M.R.; Taiebi-Rahni, M.; Farahani, M. & Heidari, M.R. (2005). Flow Measurements around a Long Axisymmetric Body with Varying Cross Section, *43rd AIAA Aerospace Sciences Meeting and Exhibit*, 10-13 January 2005, Reno, Nevada

Sorenson, R.L. & McCann, K.M. (1990). A Method for Interactive Specification of Multiple-Block Topologies, AIAA-91-0147

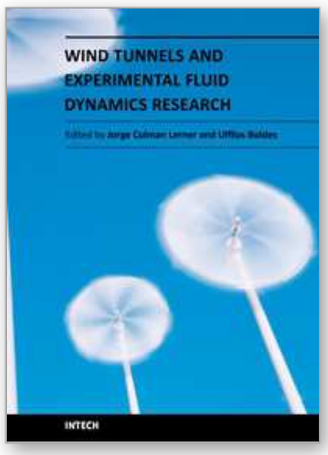

Wind Tunnels and Experimental Fluid Dynamics Research

Edited by Prof. Jorge Colman Lerner

ISBN 978-953-307-623-2
Hard cover, 709 pages
Publisher InTech
Published online 27, July, 2011
Published in print edition July, 2011

The book â€œWind Tunnels and Experimental Fluid Dynamics Researchâ€ is comprised of 33 chapters divided in five sections. The first 12 chapters discuss wind tunnel facilities and experiments in incompressible flow, while the next seven chapters deal with building dynamics, flow control and fluid mechanics. Third section of the book is dedicated to chapters discussing aerodynamic field measurements and real full scale analysis (chapters 20-22). Chapters in the last two sections deal with turbulent structure analysis (chapters 23-25) and wind tunnels in compressible flow (chapters 26-33). Contributions from a large number of international experts make this publication a highly valuable resource in wind tunnels and fluid dynamics field of research.

How to reference

In order to correctly reference this scholarly work, feel free to copy and paste the following:

M.R. Heidari, M. Farahani, M.R. Soltani and M. Taeibi-Rahni (2011). Investigations of Supersonic Flow around a Long Axisymmetric Body, Wind Tunnels and Experimental Fluid Dynamics Research, Prof. Jorge Colman Lerner (Ed.), ISBN: 978-953-307-623-2, InTech, Available from: http://www.intechopen.com/books/wind-tunnels-and-experimental-fluid-dynamics-research/investigations-of-supersonic-flow-around-a-long-axisymmetric-body

INTECH
open science | open minds

InTech Europe
University Campus STeP Ri
Slavka Krautzeka 83/A
51000 Rijeka, Croatia
Phone: +385 (51) 770 447
Fax: +385 (51) 686 166
www.intechopen.com

InTech China
Unit 405, Office Block, Hotel Equatorial Shanghai
No.65, Yan An Road (West), Shanghai, 200040, China
中国上海市延安西路65号上海国际贵都大饭店办公楼405单元
Phone: +86-21-62489820
Fax: +86-21-62489821

IntechOpen